Int. J. Heat Mass Transfer. Vol. 35, No. 6, pp. 1427–1439, 1992
Printed in Great Britain

0017–9310/92 $5.00 + 0.00

Three-dimensional boundary element thermal shape sensitivity analysis

K. GURU PRASAD and J. H. KANE
Mechanical and Aeronautical Engineering, Clarkson University, Potsdam, NY 13699, U.S.A.

(*Received* 14 *August* 1990 *and in final form* 4 *June* 1991)

Abstract—A computationally efficient and accurate shape design sensitivity analysis (DSA) approach for the thermal response of three-dimensional (3D) solid objects is presented which utilizes a direct, singular, boundary element analysis (BEA) formulation. The theoretical formulations for the primary response (the surface temperature and normal heat flux) sensitivities and the secondary response (tangential components of the heat flux, vector, interior point temperature and heat flux vector components) sensitivities are presented. A number of computational issues related to the overall efficiency of implementation of these formulations are discussed. Numerical results are presented to demonstrate the accuracy and efficiency of this approach.

INTRODUCTION

SHAPE OPTIMIZATION algorithms require knowledge of the variation of the response of the object under consideration when the parameters controlling its shape (design variables) change. Design sensitivity analysis (DSA) refers to the process of computing rates of change of response quantities associated with an object under a given set of boundary conditions, with respect to changes in these parameters. These rates of change (*sensitivities*) are then used in shape optimization by the numerical optimization procedure to determine effective search steps, regarding both direction and magnitude in the space of the design variables. In order for three-dimensional (3D) shape optimization for large problems to be tractable, it is necessary to have an accurate and computationally economical DSA. Implicit differentiation [1–9] of the discretized boundary integral equations has been shown to be an effective strategy for the formulation of DSA relations in 2D linear heat transfer and stress analysis. The major advantage of this approach lies in the fact that the LU factorization of the BEA matrix, formed during the analysis, is multiply reused in this process. Kane [1, 3] and Kane and Saigal [2, 8] have demonstrated that implicit differentiation of the discretized 2D boundary integral equations provides an effective strategy for determination of surface displacement and traction component sensitivities. In subsequent publications involving 2D boundary element DSA, they have treated axisymmetric solids [4], thermoelastic problems with body forces [10], coupled problems [11], developed both a semi-analytical [5] and a simultaneous [6] algorithm for DSA providing significant improvements in computational efficiency, and have shown that sensitivity analysis can be performed in conjunction with boundary element substructuring [7]. Recently, for 2D thermal problems with nonlinear boundary conditions [9] and temperature-dependent conductivity [12], the solution of the nonlinear discretized boundary integral equations for sensitivity analysis was accomplished by iterative procedures. For these nonlinear problems, multi-zone analysis and zone condensation strategies were shown to provide substantial computational economies for models with either localized nonlinear boundary conditions or regions of geometric insensitivity to design variables.

The 3D shape DSA formulation is identical to its 2D counterpart at the matrix level. This paper will therefore focus mainly on the distinctive new aspects that are introduced due to the 3D character of the BEA approach employed. A theoretical formulation for the entries in the matrix sensitivities required in the implicit differentiation approach is given that includes sensitivities of 3D fundamental temperature and normal heat flux solutions, unit normal vectors, and boundary element Jacobians. This formulation employs quadratic isoparametric boundary elements, and is sufficient for the computation of the sensitivities of unknown boundary temperature and normal heat flux components on the surface of the BEA model. These matrix sensitivities are shown to exhibit significant sparsity for objects with partial geometric sensitivity. The exploitation of this sensitivity is shown to yield considerable savings in computation. A formulation for the recovery of sensitivities of tangential heat flux components on the surface of the model that do not form a part of the primary response and that do not require any additional numerical integration is presented. Formulae for the recovery of temperature and heat flux vector components at interior points are also presented. A series of example problems are presented for which analytical sensitivity formulae exist. Computed sensitivities are compared to these analytic sensitivities and CPU timings are reported.

NOMENCLATURE

$[A]$ square left hand side coefficient matrix present in BEA after application of boundary conditions
a_i intrinsic element coordinates
$\{b\}$ right hand side column vector present in BEA overall system equations
b_i component of unit tangent vector used in surface tangential heat flux recovery
c jump term coefficient present in temperature boundary integral equation
D_i BEA kernel function used in internal point heat flux recovery
d_i coordinate of the source point employed in BEA fundamental solutions
e_{ijk} permutation tensor
$[F]$ square left hand side coefficient matrix present in BEA before application of boundary conditions
f arbitrary function used in Green's second identity
$[G]$ rectangular right hand side coefficient matrix present in BEA before application of boundary conditions
g suface Jacobian relating actual element and intrinsic element differential areas
g arbitrary function used in Green's second identity
$\{H\}$ row vector of element interpolation functions
$h^{(n)}$ element interpolation function associated with node n
$[J]$ second Jacobian matrix associated with surface tangential heat flux recovery
k thermal conductivity
k_i constants, used for convenience
L design variable number
l_{ij} direction cosines associated with a local coordinate system used for surface tangential heat flux recovery
n_i component of element surface unit normal vector at a point
p_i component of the heat flux vector in the local coordinate system
q^* BEA normal heat flux fundamental solution
q_i component of the heat flux vector
$\{q\}$ column vector of node point normal heat flux components before the application of boundary conditions. After application, this vector contains specified values of node point boundary conditions
S_i BEA kernal function used in internal point heat flux recovery
T^* BEA temperature fundamental solution
T temperature
$\{t\}$ column vector of node point temperatures before the application of boundary conditions. After application, this vector contains unknown values of node point boundary response quantities
X_L design variable number L
x_i coordinate of surface sample point in BEA formulation
y_i difference in sample point and source point coordinates
z_i coordinate of sample point in local coordinate system.

Greek symbols

Γ boundary
δ Dirac delta function
ρ distance from source point to sample point in BEA formulation
τ_i component of unit tangent vector used in surface tangential heat flux recovery
Ω domain.

BOUNDARY FORMULATION OF THE CONDUCTION PROBLEM

A three-dimensional isoparametric thermal BEA formulation [14–16] is discussed to set out the notation and terminology used throughout. In thermal BEA, the fundamental solution T^* refers to the temperature response of an infinite conducting medium, with conductivity k, to a unit point source of thermal energy. This point source at location $\mathbf{d}$ is represented by a Dirac delta function $\delta(\mathbf{x}-\mathbf{d})$ at sample point $\mathbf{x}$. A governing boundary integral equation can be developed by substituting T^* for 'g' in Green's second identity, shown below, and choosing 'f' to be the temperature response of the actual problem under consideration. Ω is the domain of the actual problem, Γ is the boundary of this domain and $\mathbf{n}$ is the unit normal vector on the surface. q^* denotes the normal component of the heat flux vector corresponding to the fundamental temperature solution. Use of the Fourier law of heat conduction has also been made in this derivation, along with the selection property of the delta function:

$$\int_\Omega \nabla^2 f g \, d\Omega - \int_\Omega \nabla^2 g f \, d\Omega = \int_\Gamma g \nabla f \cdot \mathbf{n} \, d\Gamma - \int_\Gamma f \nabla g \cdot \mathbf{n} \, d\Gamma \quad (1)$$

$$\nabla^2 T^* = -\frac{1}{4\pi k}\delta(\mathbf{x}-\mathbf{d}) \tag{2}$$

$$cT(d)+\int_\Gamma q^* T\,d\Gamma = \int_\Gamma T^* q\,d\Gamma. \tag{3}$$

Equation (3) can be discretized by breaking the surface of the object under consideration into boundary elements and approximating the geometry, boundary conditions, and unknown response using simple interpolating functions and the values of these quantities at a finite number of nodes:

$$cT(\mathbf{d})+\sum_{E=1}^{NEL}\left\{\int_0^1\int_0^{1-a_2} q^*\{H\}g\,da_1\,da_2\right\}^{(E)}\{T\}^{(E)} = \sum_{E=1}^{NEL}\left\{\int_0^1\int_0^{1-a_2} T^*\{H\}g\,da_1\,da_2\right\}^{(E)}\{q\}^{(E)}. \tag{4}$$

$\{H\}$ is a row vector of element interpolation functions associated with each node on element E, 'a_i' are element intrinsic coordinates, and g is the Jacobian of the transformation from the actual coordinate system to the element's intrinsic coordinate system. $\{T\}^{(E)}$ and $\{q\}^{(E)}$ are column vectors of node point temperatures and normal heat flux components respectively for element E and have been taken outside the integrals shown to produce an algebraic expression. This boundary integral equation can be written for any location of the source point of the fundamental solution. A singular boundary element formulation is obtained by locating this source point at each of the nodes present in the boundary element model, producing a square system of algebraic equations:

$$[F]\{t\} = [G]\{q\}. \tag{5}$$

$\{t\}$ is a column vector of nodal point temperatures and $\{q\}$ is a column vector of nodal point normal heat flux components. The $\{t\}$ vector has an entry for each node in the overall problem, while the $\{q\}$ vector may have additional entries if jumps in the normal component of the heat flux occur at any node. The matrix $[F]$ is square and $[G]$ is either square or rectangular.

In a well posed boundary value problem, half of the temperature and normal heat flux components will be specified (and therefore known) and the other half will be unknown. Transferring all known values in the vector $\{q\}$, placing all unknown temperature and normal heat flux components in the vector $\{t\}$, exchanging corresponding columns of the respective rectangular matrices, and performing the indicated matrix–vector multiplication on the right hand side, a solvable system of equations can be produced:

$$[A]\{x\} = \{b\}. \tag{6}$$

This matrix equation is generally solved by a direct method consisting of the triangular factorization of the matrix $[A]$ using a Gauss elimination procedure with partial pivoting, followed by forward reduction of $\{b\}$ and backward substitution to determine the unknown response vector $\{x\}$. Note that the notation has been generalized to mean that the vector $\{t\}$ is the vector of unknown boundary response quantities, while $\{q\}$ denotes the vector of specified boundary conditions in the problem. At each node, if q has been specified, then $\{t\}$ contains T for this node. If, on the other hand, T had been specified for this node, then $\{t\}$ contains q for this entry.

SENSITIVITY FORMULATION FOR SURFACE TEMPERATURE AND NORMAL HEAT FLUX COMPONENTS

As shown in refs. [1, 2], implicit differentiation of the algebraic system equations that result when the discretized boundary integral equations are written for a set of load point locations corresponding to boundary element nodes yields

$$\frac{\partial}{\partial X_L}([F]\{t\} = [G]\{q\}) \tag{7}$$

or

$$[F]\{t\}_{,L} = ([G]_{,L}\{q\} - [F]_{,L}\{t\}) \tag{8}$$

where $[F]$ and $[G]$ are BEA coefficient matrices corresponding to the column vectors of nodal point unknown response components in $\{t\}$ and specified boundary conditions in $\{q\}$ respectively. Note that the vector $\{t\}$ will contain temperatures of the nodes with specified heat flux boundary condition and $\{q\}$ will contain normal heat flux components at nodes where temperatures are specified. In the above expression, X_L represents the Lth design variable. Equation (8) reveals a fundamental characteristic of the implicit differentiation approach to DSA. If the right hand side vector shown can be formed, then the unknown nodal response sensitivity vector $\{t\}_{,L}$ can be determined by simply solving equation (8), by forward reduction and back substitution, using the factorization of the left hand side matrix $[F]$ computed in the previous analysis step.

The entries in the matrix sensitivities shown in equation (8) are assembled from contributions associated with pairs of elements and load points as

$$[F]_{,L}^{(E,P)} = \int_0^1\int_0^{1-a_2}(q^*_{,L}\{H\}g + q\{H\}g_{,L})\,da_1\,da_2 \tag{9}$$

and

$$[G]_{,L}^{(E,P)} = \int_0^1\int_0^{1-a_2}(t^*_{,L}\{H\}g + t\{H\}g_{,L})\,da_1\,da_2. \tag{10}$$

t^* and q^* are the fundamental solutions for the temperature and normal heat flux respectively, for the heat transfer problem for element E due to unit source of heat at load point P. Accordingly, $t^*_{,L}$ and $q^*_{,L}$ are

sensitivities of the fundamental temperature and normal heat flux respectively. $g_{,L}$ is the sensitivity of the determinant of the Jacobian matrix for the transformation from the intrinsic (isoparametric) coordinates a_i to the real element coordinates x_i, for example, as shown for the six-noded triangular element in Fig. 1. $\{H\}$ is a 1×6 row matrix of interpolation (shape) functions $h^{(n)}$ for the six-node isoparametric element. Sensitivity expressions for these quantities are

$$t^*_{,L} = -k_1\rho^{-2}\rho_{,L} \tag{11}$$

and

$$q^*_{,L} = k_2[\rho^{-3}(y_i n_{i,L}+n_i y_{i,L})-3y_i n_i\rho^{-4}\rho_{,L}] \tag{12}$$

where

$$k_1 = \frac{1}{4\pi K};\quad k_2 = \frac{1}{4\pi} \tag{13}$$

and

$$\rho = (y_k y_k)^{1/2} \tag{14}$$

$$\rho_{,i} = y_i\rho^{-1} \tag{15}$$

$$\rho_{,L} = y_k y_{k,L}\rho^{-1} \tag{16}$$

$$\rho_{,iL} = y_{i,L}\rho^{-1}-\rho^{-3}y_i y_k y_{k,L} \tag{17}$$

$$y_{i,L} = x_{i,L}-d_{i,L}; \tag{18}$$

also

$$n_{i,L} = g_{i,L}g^{-1}-g_i g^{-2}g_{,L} \tag{19}$$

where

$$g_{,L} = g^{-1}g_k g_{k,L} \tag{20}$$

$$g_{i,L} = e_{ijk}(x_{j,1L}x_{k,2}+x_{j,1}x_{k,2L}) \tag{21}$$

$$x_{j,1L} = \sum_{n=1}^{6}\frac{\partial h^{(n)}}{\partial a_1}x_{j,L};\quad x_{j,2L} = \sum_{n=1}^{6}\frac{\partial h^{(n)}}{\partial a_2}x_{j,L}. \tag{22}$$

In these expressions, ρ is the distance from the load point **d** to the sample point **x**, **n** is the unit outward normal to the surface at **x**, and K is the thermal conductivity of the material.

One might suspect that the differentiation of the fundamental solutions present in the BEA formulation would lead to the development of integral equations for DSA that were more singular than the original ones. This is not the case. Examination of equations (9)–(18) reveals that the functions involved in the DSA formulation have exactly the same singularity characteristics as those present in the original analysis step. That is, $t^*_{,L}$ and $q^*_{,L}$ contain functions that behave like ρ^{-1} and ρ^{-2} respectively, as this distance approaches zero. This fact allows numerical integration techniques [13] (sets of sample points and associated weighting coefficients), developed for BEA, to be employed in this DSA step without modification. This statement is true for both the outside integration (ρ never becomes zero for a particular E, P combination) and inside integration (ρ becomes zero for a particular E, P combination) processes.

The numerical integration process indicated in equations (9) and (10) deserves some further comment. These two term expressions, at first, appear to be considerably more computationally burdensome than their counterparts in BEA. Examination of Fig. 2, however, reveals that this is not the case. This figure presents the details of the hierarchical algorithm for the performance of the above-mentioned integrations in DSA. Steps preceded with the symbol **x** indicate the steps that are *extra* when compared with an analogous procedure in standard BEA. Note that only the steps associated with the computation of sensitivities of fundamental solutions and the sensitivity of the Jacobian and normals are extra. Also, even in these formulae, about half of the quantities present are not sensitivities. Note further that the arithmetic operations associated with the formation of the 1×6 matrix products remain identical to the operations utilized in standard BEA. For problems in which a significant portion of the surface is geometrically insensitive to the design variable, significant savings in computational effort can be accomplished in this DSA integration step, due to the fact that the matrix sensitivities will be sparse. Again, Fig. 2 can be used to gain an appreciation of this concept. In several places in this algorithm, tests are made to determine if certain quantities involved in the overall computation are known to be zero, and these operations are appro-

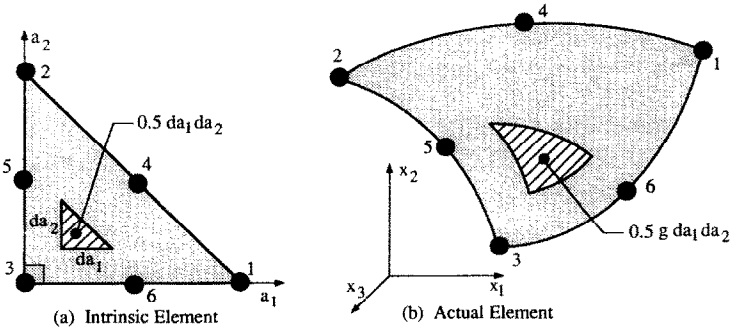

FIG. 1. Six-node isoparametric triangular boundary element.

```
      form k1 & k2
      for each E
            if both E and all P's are geometrically insensitive to XL
                  then go to skip1
c     compute (once) element geometric data at all integration points
            form x*i g*i g & ni
            if E is geometrically insensitive to XL then go to skip2
c     compute (once) element geometric sensitivity data at all integration points
x           form x*iL g*iL gL & niL
skip2:      continue
            for each P
c     compute geometric data at all integration points associated with P
                  form yi ρ ρ*i
                  if both E and this P are geometrically insensitive to XL
                  then go to skip1
                  if P is geometrically insensitive to XL
                  then go to skip3
c     compute geometric sensitivity data at all integration points associated with P
x                 form y*iL ρ*L ρ*iL
skip3:            continue
c     compute fundamental solutions at all integration points
                  form t* & q*
c     compute sensitivities of fundamental solutions at all integration points
x                 form t*,L & q*,L
c     form augmented fundamental solution times weight at all integration points
x                 form T <== (t*,L * g + t* * g,L) * w
x                 form Q <== (q*,L * g + q* * g,L) * w
c     perform matrix product & 1 x 6 sum required for all integration points
                  form [F](E,P) = [F](E,P) + Q [H]
                  form [G](E,P) = [G](E,P) + T [H]
                  next P
            next E
skip1:      continue
      return
      end
```

FIG. 2. Numerical integration algorithm for entries in matrix sensitivities.

priately bypassed. In subsequent sections, numerical examples will be presented to demonstrate these assertions regarding computational efficiency.

SENSITIVITY FORMULATION FOR SURFACE HEAT FLUX COMPONENTS

As depicted in equations (7) and (8), the quantities involved in this DSA formulation at the algebraic equation solving level are sensitivities of node point temperature and normal heat flux. In many practical problems, in-plane heat flux components that are not a part of the primary response are important. In this paper, these will be referred to as *tangential* heat flux components. Development of a sensitivity formulation for these tangential heat flux components is thus a requirement for any DSA capability for use in practical shape optimization systems. The formulae for recovery of tangential heat flux components on the surface of a BEA model can be differentiated with respect to X_L to generate a sensitivity formulation. Care must be taken to recognize all of the possible geometric and thermal quantities that can be sensitive to the design variable, and to include these derivatives in this differentiation process.

Figure 3 can be used to visualize the coordinate systems involved in the tangential heat flux components recovery and subsequent sensitivity recovery process. The global coordinate system is denoted by x_i. In the local (tangential and normal) z_i coordinate system, located at the node where tangential components of heat flux are to be recovered, p_i is used to

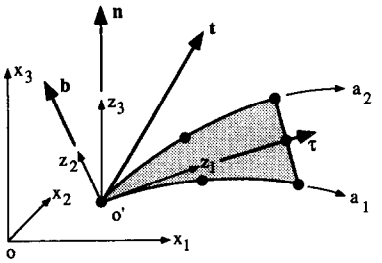

FIG. 3. Coordinate systems involved in tangential heat flux recovery.

symbolize these components (q_i is used to denote the corresponding quantities in the global directions). This local coordinate system is configured so that the z_1 direction is tangential to the boundary element and pointing in the direction of increasing a_1, z_3 is normal to the element, and z_2 is perpendicular to z_1 and z_3. In this local coordinate system, the following relationships exist:

$$p_i = -K\frac{\partial T}{\partial z_i} \tag{23}$$

$$\frac{\partial T}{\partial z_i} = [J]^{-1}\frac{\partial T}{\partial a_i} \tag{24}$$

$$q_i = l_{ji}p_j. \tag{25}$$

Letting

$$\{T\}_{,z} = \begin{Bmatrix} T_{,1} \\ T_{,2} \end{Bmatrix}; \quad \{T\}_{,a} = \begin{Bmatrix} T_{,a_1} \\ T_{,a_2} \end{Bmatrix}$$

$$\{T\}_{,zL} = \begin{Bmatrix} T_{,1L} \\ T_{,2L} \end{Bmatrix}; \quad \{T\}_{,aL} = \begin{Bmatrix} T_{,a_1L} \\ T_{,a_2L} \end{Bmatrix};$$

$$[J] = \begin{bmatrix} z_{1,a_1} & z_{2,a_1} \\ z_{1,a_2} & z_{2,a_2} \end{bmatrix} \tag{26}$$

then

$$\{p_i\}_{,L} = -K[[J]_{,L}^{-1}\{T\}_{,a} + [J]^{-1}\{T\}_{,aL}] \tag{27}$$

where

$$[J]_{,L}^{-1} = [J]_{,L}^{A}|J|^{-1} - [J]^{A}|J|^{-2}[J]_{,L} \tag{28}$$

and

$$[J] = \begin{bmatrix} j_{11} & j_{12} \\ j_{21} & j_{22} \end{bmatrix}; \quad [J]^{A} = \begin{bmatrix} j_{22} & -j_{21} \\ -j_{12} & j_{11} \end{bmatrix};$$

$$|J| = j_{11}j_{22} - j_{12}j_{21} \tag{29}$$

$$[J]_{,L} = \begin{bmatrix} j_{11,L} & j_{12,L} \\ j_{21,L} & j_{22,L} \end{bmatrix}; \quad [J]_{,L}^{A} = \begin{bmatrix} j_{22,L} & -j_{21,L} \\ -j_{12,L} & j_{11,L} \end{bmatrix} \tag{30}$$

$$|J|_{,L} = j_{11,L}j_{22} + j_{11}j_{22,L} - (j_{12,L}j_{21} + j_{12}j_{21,L}) \tag{31}$$

$$j_{km} = z_{m,a_k} = \sum_{n=1}^{6} \frac{\partial h^{(n)}}{\partial a_k} z_m^{(n)}; \tag{32}$$

$$j_{km,L} = (z_{m,a_k})_{,L} = \sum_{n=1}^{6} \frac{\partial h^{(n)}}{\partial a_k} z_{m,L}^{(n)}.$$

It is important to recognize that all of the vector components shown above are resolved in the local coordinate system. The transformations of the components of these physical entities from the global coordinate system are

$$z_{r,L} = l_{ri,L}x_i + l_{ri}x_{i,L}; \quad p_{r,L} = l_{ri,L}q_i + l_{ri}q_{i,L} \tag{33}$$

where

$$l_{i1} = \tau_i; \quad l_{i2} = b_i; \quad l_{i3} = n_i; \quad \text{and} \tag{34}$$

$$l_{i1,L} = \tau_{i,L}; \quad l_{i2,L} = b_{i,L}; \quad l_{i3,L} = n_{i,L}$$

$$\tau_i = \tau^{-1}x_{i,a_1}; \quad \tau_{i,L} = -\tau^{-2}\tau_{,L}x_{i,a_1} + \tau^{-1}x_{i,a_1L} \tag{35}$$

$$\tau = (x_{1,a_1}^2 + x_{2,a_1}^2 + x_{3,a_1}^2)^{1/2}; \tag{36}$$

$$\tau_{,L} = \tau^{-1}(x_{1,a_1}x_{1,a_1L} + x_{2,a_1}x_{2,a_1L} + x_{3,a_1}x_{3,a_1L})$$

$$x_{i,a_1} = \sum_{n=1}^{6} \frac{\partial h^{(n)}}{\partial a_1} x_i^{(n)}; \quad x_{i,a_1L} = \sum_{n=1}^{6} \frac{\partial h^{(n)}}{\partial a_1} x_{i,L}^{(n)} \tag{37}$$

$$b_i = e_{ijk}n_j\tau_k; \quad b_{i,L} = e_{ijk}(n_{j,L}\tau_k + n_j\tau_{k,L}). \tag{38}$$

Recall that $n_{i,L}$ has been defined in equation (19). This completes the tangential heat flux component sensitivity analysis formulation in the local coordinate system. To obtain the sensitivities of the complete heat flux vector in the global coordinate system, one needs to differentiate the vector component transformation law to obtain

$$q_{i,L} = l_{ji,L}p_j + l_{ji}p_{j,L}. \tag{39}$$

INTERIOR POINT SENSITIVITY ANALYSIS

Integral relations are well known for the recovery of temperature and heat flux vector components at sample points in the domain (interior) of a BEA model. These integral equations can be differentiated to yield new integral equations for the recovery of the sensitivities of temperature and heat flux components to the design variable. The integral equations that result involve the boundary response (nodal temperature and normal heat flux) and the sensitivity of these response quantities. Thus, the recovery of internal point sensitivities can be accomplished via a boundary integration process completely analogous to that performed in the original BEA process. This formulation is shown below. In this formulation, indicial notation is employed instead of the matrix notation shown, for example, in equations (9) and (10), in order to conveniently express relations involving the vectors present in the integral equation for internal point response recovery:

$$\begin{aligned} T_{,L}(\mathbf{d}) = &\sum_{E=1}^{NE}\left[\sum_{n=1}^{6}\left(\int_0^1\int_0^{1-a_2}[q_{,L}^{*}h^{(n)}g + q^{*}h^{(n)}g_{,L}]\,da_1\,da_2\right)t^{(n)}\right]^{(E)} \\ &-\sum_{E=1}^{NE}\left[\sum_{n=1}^{6}\left(\int_0^1\int_0^{1-a_2}[t_{,L}^{*}h^{(n)}g + t^{*}h^{(n)}g_{,L}]\,da_1\,da_2\right)q^{(n)}\right]^{(E)} \\ &+\sum_{E=1}^{NE}\left[\sum_{n=1}^{6}\left(\int_0^1\int_0^{1-a_2}q^{*}h^{(n)}g\,da_1\,da_2\right)t_{,L}^{(n)}\right]^{(E)} \\ &-\sum_{E=1}^{NE}\left[\sum_{n=1}^{6}\left(\int_0^1\int_0^{1-a_2}t^{*}h^{(n)}g\,da_1\,da_2\right)q_{,L}^{(n)}\right]^{(E)} \end{aligned} \tag{40}$$

$$\begin{aligned} -\frac{q_{i,L}(\mathbf{d})}{K} = &\sum_{E=1}^{NE}\left[\sum_{n=1}^{6}\left(\int_0^1\int_0^{1-a_2}[D_{i,L}h^{(n)}g + D_ih^{(n)}g_{,L}]\,da_1\,da_2\right)t^{(n)}\right]^{(E)} \\ &-\sum_{E=1}^{NE}\left[\sum_{n=1}^{6}\left(\int_0^1\int_0^{1-a_2}[S_{i,L}h^{(n)}g + S_ih^{(n)}g_{,L}]\,da_1\,da_2\right)q^{(n)}\right]^{(E)} \\ &+\sum_{E=1}^{NE}\left[\sum_{n=1}^{6}\left(\int_0^1\int_0^{1-a_2}D_ih^{(n)}g\,da_1\,da_2\right)t_{,L}^{(n)}\right]^{(E)} \\ &-\sum_{E=1}^{NE}\left[\sum_{n=1}^{6}\left(\int_0^1\int_0^{1-a_2}S_ih^{(n)}g\,da_1\,da_2\right)q_{,L}^{(n)}\right]^{(E)}. \end{aligned} \tag{41}$$

All of the quantities in equations (40) and (41) have been defined, except for the vectors D_i and S_i and their sensitivities. These are given as

$$D_i = -k_2\rho^{-3}[3(y_in_i)\rho^{-1}\rho_{,i} + n_i] \tag{42}$$

$$S_i = -k_1\rho^{-2}\rho_{,i} \tag{43}$$

$$\begin{aligned} D_{i,L} = k_2\rho^{-3}[&-3(y_in_i)_{,L}\rho^{-1}\rho_{,i} - 3(y_in_i)\rho^{-1}\rho_{,iL} \\ &+12(y_in_i)\rho^{-2}\rho_{,L}\rho_{,i} - n_{i,L} + 3\rho^{-1}\rho_{,L}n_{iL}] \end{aligned} \tag{44}$$

$$S_{i,L} = k_1\rho^{-2}[2\rho^{-1}\rho_{,L}\rho_{,i} - \rho_{,iL}]. \tag{45}$$

Again, one might suspect that the differentiation of the fundamental solutions undertaken in the interior point sensitivity formulation would lead to the development of integral equations that are more singular than the corresponding original ones. As mentioned earlier, however, this is not the case. Examination of equations (44), (45), and (14)–(18) reveals that the functions involved in this interior point DSA formulation have exactly the same singularity characteristics as those present in the original analysis step. Thus, numerical integration techniques developed for recovery of interior point response information in standard BEA can be employed in this DSA step without modification. The numerical integration pro-

cess indicated in equations (40) and (41) appears to be considerably more computationally burdensome than the corresponding operation in BEA. A figure similar to Fig. 2 could be constructed, for example, to illustrate that this is not *entirely* the case. One could argue that about twice the computational work would be required in this process, compared to interior point response recovery in the original BEA, due to the fact that both the surface response and its sensitivity are involved in the computation. Closer examination of the last two terms in either equation (40) or (41), however, reveals an interesting characteristic. The integrations indicated in these terms are exactly the same integrations that would be performed in the original BEA internal point response recovery process. Thus, if these coefficients are saved and reused in the DSA step, their recomputation can be avoided. For problems in which a significant portion of the surface is geometrically insensitive to the design variable, significant savings in computational effort can again be accomplished in this DSA integration step for interior point response, due to the fact that many of the terms in equations (40) and (41) will be zero for a significant number of the elements comprising the overall BEA model.

EXAMPLE PROBLEMS

A series of example problems is presented in order to demonstrate the accuracy and efficiency of the formulation presented above. All these problems were run on the same dedicated computer system with a UNIX operating system using the same Fortran 77 compiler and compiler options.

Table 1. Surface temperature and normal heat flux sensitivities for a rectangular bar

	Exact		Computed	
Point	$t_{,L}$	$q_{,L}$	$t_{,L}$	$q_{,L}$
1	0.0	675.00	0.00000	675.87
3	0.0	0.00	0.01365	0.00
5	0.0	0.00	0.00067	0.00
7	0.0	0.00	−0.02284	0.00
9	0.0	−675.00	0.00000	−667.97
12	0.0	0.00	−0.00153	0.00
14	0.0	0.00	−0.00757	0.00
16	0.0	0.00	−0.01669	0.00
19	0.0	675.00	0.00000	672.69
30	0.0	0.00	0.00153	0.00
32	0.0	0.00	−0.00767	0.00
34	0.0	0.00	−0.01374	0.00
37	0.0	675.00	0.00000	668.63

Rectangular bar example

To start with, the problem of a rectangular bar under pure axial heat flow was studied. Figure 4 shows the geometry, boundary conditions and geometric sensitivity of the nodes present in this one zone BEA model, with 80 six-noded triangular elements and containing 162 nodes. The coefficient of thermal conductivity was taken as 3 units. The computer storage required for this problem to take it through the sensitivity analysis (including internal point response recovery at six selected points) was 145 605 words. Tables 1–3 summarize the results of the runs made with this model. In this example problem, the development of an analytical solution for the various response sensitivities was straightforward. The nodes

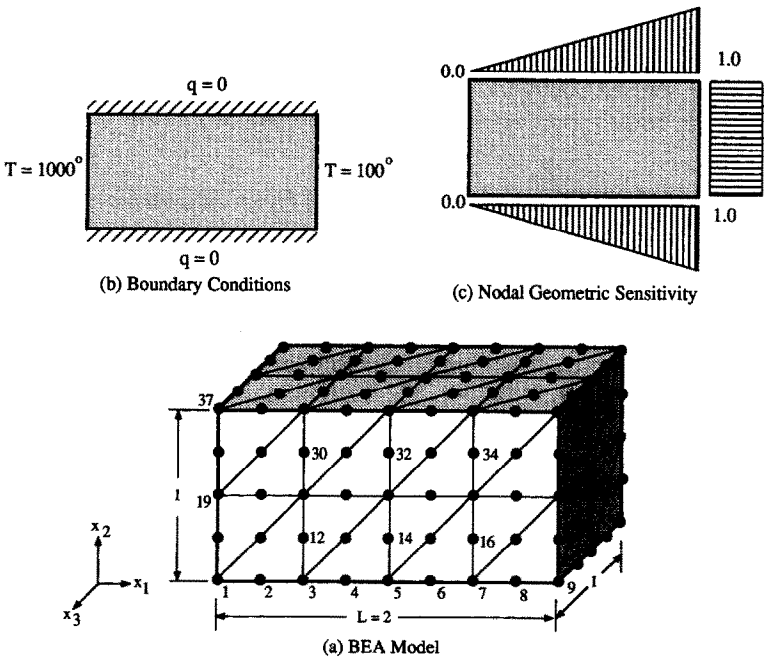

FIG. 4. Rectangular bar example problem.

Table 2. Surface tangential heat flux sensitivities for a rectangular bar

	Exact		Computed	
Point	$q_{1,L}$	$q_{2,L}$	$q_{1,L}$	$q_{2,L}$
1	−675.00	0.0000	−675.51	0.0000
3	−675.00	0.0000	−675.00	0.4003
5	−675.00	0.0000	−674.82	0.2161
7	−675.00	0.0000	−674.31	−0.0834
9	−675.00	0.0000	−675.75	0.0000
12	−675.00	0.0000	−674.82	−0.0358
14	−675.00	0.0000	−674.78	−0.0182
16	−675.00	0.0000	−674.29	−0.0642
19	−675.00	0.0000	−675.70	0.0000
30	−675.00	0.0000	−674.87	−0.0388
32	−675.00	0.0000	−674.88	0.0056
34	−675.00	0.0000	−674.51	−0.0106
37	−675.00	0.0000	−676.31	0.0000

in the model have an X_1 geometric sensitivity to the length design variable $X_L = L$ that varies linearly from zero at the left end to unity at the right end. Therefore, the node point temperature sensitivities have to be zero. This is true because the length change causes a temperature change, but the nodes move to new locations that are at the same temperature as they were in the original design. Analytical and computed surface response sensitivities are shown in Table 1 for the group of node points illustrated in Fig. 4. Note that the computed solutions for these sensitivities are all zero within acceptable limits of accuracy. Also, the nonzero values of normal heat flux sensitivity show that the computed values have a very good agreement with analytical values with a maximum error of about 1%. Surface tangential heat flux sensitivities along the global 1 direction are presented in Table 2. This table reveals that the computed values have extremely good accuracy, with about 0.2% error in the worst case. Table 3 shows interior sample point response sensitivities for a set of six selected points for the case where these points have linearly varying geometric

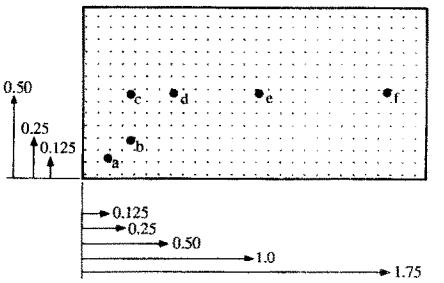

FIG. 5. Location of internal points in a rectangular bar.

sensitivities (just like temperature) and also where these points have zero geometric sensitivity. This latter case was done to demonstrate the case involving nonzero temperature sensitivities. As shown in Fig. 5, these sample points are chosen such that they cover the entire region inside the bar starting from very close to the boundary and going up to the center of the model. All points are in the midplane of the bar along the 3 direction (i.e. $z = -0.5$). Note the accuracy of these predictions at the points closest to the surface provided by this theoretical formulation. These quantities were computed using customized 'near integration' rules that cluster integration sample points near locations where the integrands experience rapid variation in their values.

Hollow cylinder example

The physical problem chosen for this second example was a thick circular hollow cylinder whose inner and outer radial surfaces were maintained at constant temperatures of 1000 and 100 units respectively. The other faces of the cylinder were insulated against heat flow. The coefficient of thermal conductivity was taken as 3 units. Figures 6(a) and (b) show the geometry and boundary conditions imposed on all of the quarter symmetry BEA models discussed. A series of analyses and design sensitivity analyses was per-

Table 3. Internal response sensitivities for a rectangular bar

	Exact				Computed			
Point	T_L	$q_{1,L}$	$q_{2,L}$	$q_{3,L}$	T_L	$q_{1,L}$	$q_{2,L}$	$q_{3,L}$
Case 1: sample points having linearly varying x_1 geometric sensitivity								
a	0.0	−675.00	0.0	0.0	0.03409	−672.80	−0.92111	−0.68729
b	0.0	−675.00	0.0	0.0	0.02584	−673.25	−0.63779	0.01813
c	0.0	−675.00	0.0	0.0	0.03639	−673.08	0.00673	0.00673
d	0.0	−675.00	0.0	0.0	0.01061	−674.84	0.01016	0.01016
e	0.0	−675.00	0.0	0.0	0.00001	−674.85	0.01228	0.01228
f	0.0	−675.00	0.0	0.0	−0.02142	−674.79	0.00673	0.00673
Case 2: points having zero geometric sensitivity								
a	28.125	−675.00	0.0	0.0	28.1340	−674.25	−2.48140	−0.04935
b	56.250	−675.00	0.0	0.0	56.2580	−674.14	−0.53671	0.79234
c	56.250	−675.00	0.0	0.0	56.2630	−674.78	0.00564	0.00564
d	112.500	−675.00	0.0	0.0	112.5000	−674.82	0.00927	0.00927
e	225.000	−675.00	0.0	0.0	224.9700	−674.86	0.01271	0.01271
f	393.500	−675.00	0.0	0.0	393.6700	−674.85	0.01901	0.01901

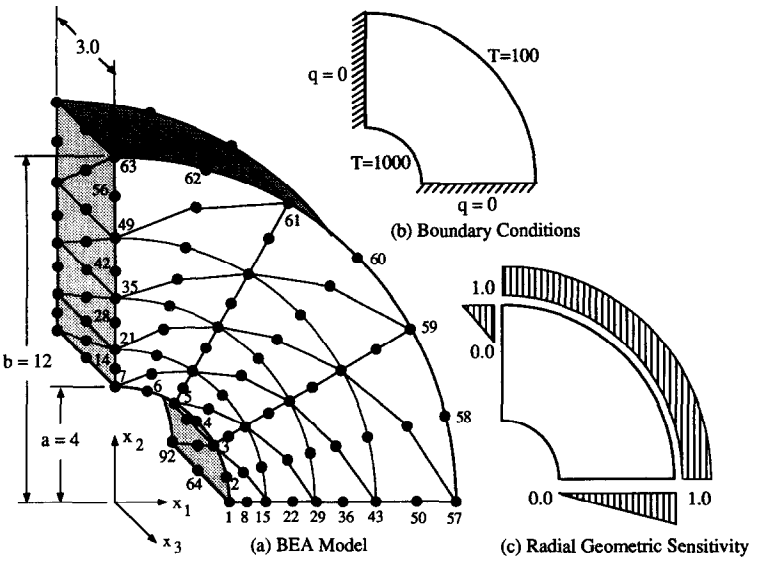

FIG. 6. Hollow cylinder example problem.

formed based upon this physical problem. In all of these cases, the outer radius b was chosen as the design variable. The analytical solution for this heat transfer problem is well known, with the temperature a logarithmic function of radius and the heat flux varying as the reciprocal of radius. These expressions for temperature and normal heat flux were differentiated to yield exact analytical expressions for these sensitivities to changes in b. It is important to note here that the derivatives computed in this implicit differentiation DSA approach are true material derivatives, including the change in the response field and the possible change in the sample point location induced by the change in the design variable. Thus, any differentiation of an exact analytical expression must also be a material differentiation, performed by first parameterizing the sample point location in the exact expression in terms of the design variable and then taking due regard for this derivative in the differentiation process. Figure 6(c), for example, shows two different schemes that can be employed to control sets of sample (node) point locations, both based upon the value of the design variable b. The *full* geometric sensitivity scheme has all nodes with radial location greater than a geometrically sensitive to b. This radial geometric sensitivity varies in a linear fashion from zero at $R = a$ to unity at $R = b$. The second scheme, also depicted in Fig. 6(c), has only the nodes in the radially outward-most row of elements geometrically sensitive to b. Note that a change in b will cause an identical change in the actual temperature and heat flow fields simulated by either the full or partially sensitive BEA models. However, because the nodes present in these two BEA models move to different locations in this response field, the node point geometric sensitivities will be different. Nodes on the inner and outer radius of these cylinder models will have identical response sensitivities because these nodes have identical geometric sensitivities in both the full and partial geometric sensitivity scheme.

Case 1: *one-zone model with full geometric sensitivity*. Figure 6(a) shows the single zone BEA model used in these demonstration problems. This model contained 154 nodes and 76 six-node triangular elements and the overall left hand side matrix associated with this model required 132 209 words of computer memory. Table 4 contains CPU timings for the major computational steps involved in both the analysis and DSA process. From this table it is seen that the 24.7 CPU seconds spent in the analysis step to factor the BEA overall system matrix is saved in the DSA process. However, the numerical integrations required in the DSA step take about twice as much time as that required in the analysis. This is due to the fact that the two term expression for the kernels shown in equations (9) and (10) is about twice as complicated as that integrated in the usual BEA process. Table 5 contains the exact and computed values of the temperature and normal heat flux sensitivities for the case of full geometric sensitivity illustrated in Fig. 6(c). Table 6 contains the exact and computed values of the tangential heat flux sensitivities, while Table 7 contains temperature and heat flux vector sensitivities for the internal points shown in Fig. 7. The internal response recovery points are all located in the $x_3 = -1.5$ plane and have radial geometric sensitivities that are the same as nodes located at the same radial locations. Note the extreme accuracy of the predictions appearing in *all* these tables, with most predictions in error less than 1%.

Case 2: *one-zone model with partial geometric sensitivity*. This BEA model is identical to the one used in the previous example except that its nodes were only partially sensitive to the design variable b.

Table 4. CPU timings for major steps in analysis and DSA for cylinder example cases

Step	Case 1	Case 2	Case 3	Case 4	Case 5
Analysis					
Preliminaries	1.4	1.4	1.5	1.8	1.7
Numerical integration	24.7	24.6	23.5	22.9	22.7
Zone assembly	3.5	3.6	4.0	2.7	2.6
Zone condensation	0.0	0.0	0.0	0.0	1.9
Overall assembly	0.1	0.1	0.1	0.1	0.1
Matrix factorization	2.2	2.2	2.2	1.7	0.2
Forward reduction and back substitution	0.3	0.3	0.3	0.4	0.2
Surface response recovery	0.4	0.4	0.3	0.5	0.0
Interior response recovery	4.8	6.2	8.2	8.4	0.0
Design sensitivity analysis					
Preliminaries	0.3	0.3	0.1	0.1	0.1
Numerical integration	48.2	21.6	42.8	10.5	10.1
Zone assembly	4.1	4.1	4.6	1.2	0.7
Overall assembly	0.1	0.1	0.1	0.0	0.0
Forward reduction and back substitution	0.3	0.3	0.3	0.4	0.2
Surface response recovery	0.3	0.3	0.3	0.3	0.0
Interior response recovery	12.0	13.0	17.0	17.9	0.0
Total	102.7	78.5	105.3	68.9	40.5

Table 4 again reveals that the 24.6 CPU seconds spent in the analysis step to factor the BEA overall system matrix are saved in the DSA process. In this example, the numerical integrations required in the DSA step take only 88% of the time required in the analysis. Although the more complicated two term expression for the kernels shown in equations (9) and (10) is again being integrated, this integration is only required for the reduced number of element and load point pairs that produce finite values of $q_{,L}$, $t^*_{,L}$ and $q^*_{,L}$, in this model with partial geometric sensitivity. Tables 8–10 contain the exact and computed values of the surface and internal response sensitivities for this case of partial geometric sensitivity illustrated in Fig. 6(c). Again, the internal stress recovery points are all located in the $x_3 = -1.5$ plane but they all have radial geometric sensitivities equal to zero. It can be seen from this

Table 5. Surface temperature and normal heat flux sensitivities for case 1

	Exact		Computed	
Point	$t_{,L}$	$q_{,L}$	$t_{,L}$	$q_{,L}$
1	0.00000	−46.6051	0.00000	−46.6520
2	0.00000	−46.6051	0.00000	−46.5890
3	0.00000	−46.6051	0.00000	−46.6180
4	0.00000	−46.6051	0.00000	−46.5850
5	0.00000	−46.6051	0.00000	−46.6240
6	0.00000	−46.6051	0.00000	−46.5960
7	0.00000	−46.6051	0.00000	−46.5640
8	−5.17260	0.0000	−5.16630	0.0000
14	−5.17260	0.0000	−5.16870	0.0000
15	−8.02380	0.0000	−8.02760	0.0000
21	−8.02380	0.0000	−8.00760	0.0000
22	−9.15290	0.0000	−9.15910	0.0000
28	−9.15290	0.0000	−9.12670	0.0000
29	−8.97350	0.0000	−8.98040	0.0000
36	−7.77990	0.0000	−7.78660	0.0000
42	−7.77990	0.0000	−7.75320	0.0000
43	−5.78630	0.0000	−5.78860	0.0000
49	−5.78630	0.0000	−5.75960	0.0000
50	−3.15270	0.0000	−3.13600	0.0000
56	−3.15270	0.0000	−3.13520	0.0000
57	0.00000	−32.6020	0.00000	−32.5750
59	0.00000	−32.6020	0.00000	−32.7860
60	0.00000	−32.6020	0.00000	−32.5690
61	0.00000	−32.6020	0.00000	−32.7660
62	0.00000	−32.6020	0.00000	−32.5960
63	0.00000	−32.6020	0.00000	−32.6020

Table 6. Surface tangential heat flux sensitivities for case 1

	Exact		Computed	
Point	$q_{1,L}$	$q_{2,L}$	$q_{1,L}$	$q_{2,L}$
1	−46.6051	0.0000	−47.8110	0.0000
2	−45.0171	−12.0624	−45.0020	−12.0580
3	−40.3612	−23.3026	−40.4730	−23.1340
4	−32.9548	−32.9548	−32.9400	−32.9400
5	−23.3026	−40.3612	−23.4870	−40.2760
6	−12.0624	−45.0171	−12.0600	−45.0080
7	0.0000	−46.6051	0.0000	−47.7480
8	−49.3842	0.0000	−48.9390	0.0000
14	0.0000	−49.3842	0.0000	−48.9780
15	−49.2023	0.0000	−49.8510	0.0000
21	0.0000	−49.2023	0.0000	−49.7620
22	−47.4179	0.0000	−47.2240	0.0000
28	0.0000	47.4179	0.0000	−47.2110
29	−44.8021	0.0000	−45.1460	0.0000
35	0.0000	−44.8021	0.0000	−45.1120
36	−41.8015	0.0000	−41.6890	0.0000
42	0.0000	−41.8015	0.0000	−41.6860
43	−38.6774	0.0000	−38.8020	0.0000
49	0.0000	−38.6774	0.0000	−38.8640
50	−35.5819	0.0000	−35.4800	0.0000
56	0.0000	−35.5819	0.0000	−35.4700
57	−32.6020	0.0000	−32.5990	0.0000
58	31.4911	−8.4380	−31.4650	−8.4311
59	−28.2342	−16.3010	−28.3220	−16.5160
60	−23.0531	−23.0531	−23.0300	−23.0300
61	−16.3010	−28.2342	−16.2600	−28.4470
62	−8.4380	−31.4911	−8.4364	−31.4850
63	0.0000	−32.6020	0.0000	−32.6870

Table 7. Internal response sensitivities for case 1

Point	Exact				Computed			
	$T_{,L}$	$q_{1,L}$	$q_{2,L}$	$q_{3,L}$	$T_{,L}$	$q_{1,L}$	$q_{2,L}$	$q_{3,L}$
a	−8.9735	−43.2755	−11.5956	0.0	−8.9752	−43.2850	−13.0410	−0.671E−5
b	−5.1726	−34.9199	−34.9199	0.0	−5.1419	−35.5740	−35.5990	−0.108E−3
c	−8.0238	−34.7913	−34.7913	0.0	−8.0175	−34.7680	−34.7980	−0.267E−3
d	−9.1529	−33.5295	−33.5295	0.0	−9.1465	−33.5140	−33.5540	0.542E−4
e	−8.9735	−31.6798	−31.6798	0.0	−8.9656	−31.6750	−31.7050	0.717E−4
f	−3.1527	−25.1602	−25.1602	0.0	−3.1482	−25.1180	−25.1590	0.576E−4
g	−8.9735	−22.4010	−38.7997	0.0	−8.9617	−22.4220	−38.8090	0.263E−3

example case that the sensitivities of the response at the internal points can be computed regardless of whether the overall model has full or partial geometric sensitivity. That is, Tables 7 and 10 demonstrate that interior response sensitivities are computable both when the internal points chosen move or do not move with respect to the unperturbed model. Note again the extreme accuracy of these predictions, with most predictions in error less than 1%.

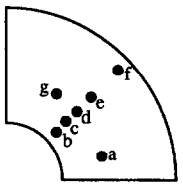

FIG. 7. Locations of internal sample points.

Case 3: *two-zone model with full geometric sensitivity*. Figure 8 shows a two-zone BEA model also used in these demonstration problems. This model contained 159 nodes (five more than the single zone model) and 88 six-node triangular elements (12 more than the single zone model) and the sparse blocked overall left hand side matrix required 133 185 words of computer memory. From Table 4 it is seen that the 24.7 CPU seconds spent in the analysis step to factor the BEA overall system matrix are saved in the DSA process. However, the numerical integrations required in the DSA step again took about twice as much time as that required in the analysis. This is again due to the fact that the two term expression for the kernels shown in equations (9) and (10) is about twice as

Table 8. Surface temperature and normal heat flux sensitivities for case 2

Point	Exact		Computed	
	$t_{,L}$	$q_{,L}$	$t_{,L}$	$q_{,L}$
1	0.00000	−46.6051	0.00000	−46.6690
2	0.00000	−46.6051	0.00000	−46.6290
3	0.00000	−46.6051	0.00000	−46.6780
4	0.00000	−46.6051	0.00000	−46.6460
5	0.00000	−46.6051	0.00000	−46.6860
6	0.00000	−46.6051	0.00000	−46.6530
7	0.00000	−46.6051	0.00000	−46.6820
8	9.87860	0.0000	9.88740	0.0000
14	9.87860	0.0000	9.88970	0.0000
15	19.22360	0.0000	19.23700	0.0000
21	19.22360	0.0000	19.23900	0.0000
22	28.13260	0.0000	28.15000	0.0000
28	28.13260	0.0000	28.15600	0.0000
29	36.68050	0.0000	36.69900	0.0000
36	44.92570	0.0000	44.94200	0.0000
42	44.92570	0.0000	44.96300	0.0000
43	52.91490	0.0000	52.91600	0.0000
49	52.91490	0.0000	52.95800	0.0000
50	24.02920	0.0000	24.06500	0.0000
56	24.02920	0.0000	24.06000	0.0000
57	0.00000	−32.6020	0.00000	−32.7750
58	0.00000	−32.6020	0.00000	−32.3660
59	0.00000	−32.6020	0.00000	−32.6260
60	0.00000	−32.6020	0.00000	−32.4040
61	0.00000	−32.6020	0.00000	−32.6080
62	0.00000	−32.6020	0.00000	−32.4300
63	0.00000	−32.6020	0.00000	−32.4520

Table 9. Surface tangential heat flux sensitivities for case 2

Point	Exact		Computed	
	$q_{1,L}$	$q_{2,L}$	$q_{1,L}$	$q_{2,L}$
1	−46.6051	0.0000	−46.6340	0.0000
2	−45.0171	−12.0624	−45.0400	−12.0690
3	−40.3612	−23.3026	−40.5260	−23.1640
4	−32.9548	−32.9548	−32.9840	−32.9840
5	−23.3026	−40.3612	−23.5180	−40.3300
6	−12.0624	−45.0171	−12.0750	−45.0640
7	0.0000	−46.6051	0.0000	−47.7480
8	−39.7550	0.0000	−39.7950	0.0000
14	0.0000	−39.7550	0.0000	−39.7990
15	−34.2043	0.0000	−34.2040	0.0000
21	0.0000	−34.2043	0.0000	−34.2700
22	−29.6358	0.0000	−29.6340	0.0000
28	0.0000	−29.6358	0.0000	−29.6500
29	−25.8271	0.0000	−25.8370	0.0000
35	0.0000	−25.8271	0.0000	−25.8760
36	−22.6178	0.0000	−22.5750	0.0000
42	0.0000	−22.6178	0.0000	−22.6180
43	−19.8890	0.0000	−19.7900	0.0000
49	0.0000	−19.8890	0.0000	−20.6850
50	−27.9045	0.0000	−27.4890	0.0000
56	0.0000	−27.9045	0.0000	−27.5090
57	−32.6020	0.0000	−32.8540	0.0000
58	−31.4911	−8.4380	−31.2630	−8.3768
59	−28.2342	−16.3010	−28.1840	−16.4350
60	−23.0531	−23.0531	−22.9130	−22.9130
61	−16.3010	−28.2342	−16.1810	−28.3100
62	−8.4380	−31.4911	−8.3936	−31.3250
63	0.0000	−32.6020	0.0000	−32.6870

Table 10. Internal response sensitivities for case 2

Point	Exact				Computed			
	$T_{,L}$	$q_{1,L}$	$q_{2,L}$	$q_{3,L}$	$T_{,L}$	$q_{1,L}$	$q_{2,L}$	$q_{3,L}$
a	36.6805	−24.9470	−6.6845	0.0	36.6790	−24.9290	−6.6867	−0.882E−3
b	9.8787	−28.1110	−28.1110	0.0	9.8853	−28.1060	−28.1180	−0.327E−3
c	19.2236	−24.1861	−24.1861	0.0	19.2310	−24.1890	−24.1980	−0.171E−3
d	28.1326	−20.9556	−20.9556	0.0	28.1420	−20.9390	−20.9640	−0.863E−4
e	36.6805	−18.2625	−18.2625	0.0	36.6890	−18.2540	−18.2620	−0.532E−4
f	60.5853	−12.4106	−12.4106	0.0	60.6860	−12.3470	−12.3400	0.112E−3
g	36.6805	−12.9135	−22.3669	0.0	36.6940	−12.9030	−22.3810	0.235E−3

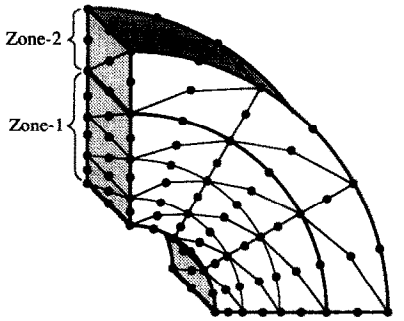

FIG. 8. Hollow cylinder two-zone BEA model.

complicated as that integrated in the usual BEA process. The accuracy of the temperature, surface heat flux components, and internal response sensitivities for this case were similar to those obtained in the single zone problem.

Case 4: two-zone model with partial geometric sensitivity. In this two-zone model, only zone 2 is geometrically sensitive to b, and thus only this zone contributes finite values of $[F]_{,L}$ and $[G]_{,L}$. This numerical integration in the DSA step takes only 46% of the time required to perform the numerical integration in the analysis. The accuracy of the temperature, surface heat flux components, and internal response sensitivities for this case were again similar to those obtained in the single zone, partially sensitive problem. This example quantifies the computer time savings that can be achieved via the implicit differentiation approach for models with partial geometric sensitivity.

Case 5: two-zone model with partial geometric sensitivity and with zone 1 condensed. This case is identical to the previous one except that zone 1 is condensed in the analysis process as described in ref. [7]. All matrices present in the DSA process for this case are of reduced size as described in this reference. The accuracies in this case are identical to those occurring in case 4.

SUMMARY

A three-dimensional design sensitivity analysis formulation has been presented based upon the boundary element analysis method and implicit differentiation. The effectiveness of this theoretical formulation and its implementation has been demonstrated for the accurate and efficient computation of the sensitivities of temperature, surface heat flux components, and internal response quantities by means of a series of three-dimensional example problems.

Acknowledgements—Portions of the research discussed herein have been supported by grants from the NASA Lewis Research Center (NAG 3-1089) and the U.S. National Science Foundation (DDM-8996171) to Clarkson University. Any opinions, findings, and conclusions or recommendations expressed in this publication are those of the authors and do not reflect the view of these other organizations.

REFERENCES

1. J. H. Kane, Shape optimization utilizing a boundary element formulation, *BETECH 86, Proc. 1986 Boundary Element Technology Conf.*, MIT (1986).
2. J. H. Kane and S. Saigal, Design sensitivity analysis of solids using BEM, *J. Engng Mech. ASCE* **114,** 1703–1722 (1988).
3. J. H. Kane, A second generation structural shape optimization capability employing a boundary element formulation, *Numeta-87, Proc.* (Edited by G. N. Pande and J. Middleton), Vol. 1, Section D43 (1987).
4. S. Saigal, J. T. Borggaard and J. H. Kane, Boundary element implicit differentiation equations for design sensitivities of axisymmetric structures. *Int. J. Solids Struct.* **25,** 527–538 (1989).
5. S. Saigal, J. H. Kane and R. Aithal, Semi-analytical structural sensitivity formulation using boundary elements, *AIAA J.* **27,** 1615–1621 (1989).
6. J. H. Kane and M. Stabinsky, Simultaneous computation of multiple sensitivities by a boundary element structural analysis formulation, *Proc. Third Int. Conf. on CAD/CAM Robotics and Factories of the Future* (1988).
7. J. H. Kane and S. Saigal, An arbitrary multi-zone condensation technique for boundary element design sensitivity analysis, *AIAA J.* **28,** 1277–1284 (1990).
8. S. Saigal and J. H. Kane, A boundary element shape optimization system for aircraft components, *AIAA J.* **28,** 1203–1204 (1990).
9. J. H. Kane and H. Wang, Boundary element shape sensitivity analysis formulations for thermal problems with nonlinear boundary conditions, *AIAA J.* **29**(5), 1978–1989 (1991).
10. J. H. Kane, B. L. K. Kumar and M. Stabinsky, Transient thermoelasticity and other body force effects on boundary element shape sensitivity analysis, *Int. J. Numer. Meth. Engng* **31,** 1203–1230 (1991).
11. J. H. Kane, Boundary element design sensitivity analysis formulations for coupled problems, *Engng Anal.* **7,** 21–32 (March 1990).

12. J. K. Kane and H. Wang, Boundary formulations for shape sensitivity of temperature dependent conductivity problems, *Int. J. Numer. Meth. Engng* (in press).
13. J. H. Kane, A. Gupta and S. Saigal, Reusable Intrinsic Sample Point (RISP) algorithm for the efficient numerical integration of three dimensional curved boundary elements, *Int. J. Numer. Meth. Engng* **28,** 1661–1676 (1989).
14. P. K. Banerjee and R. Butterfield, *Boundary Element Methods in Engineering Science*. McGraw-Hill, London (1981).
15. C. A. Brebbia and S. Walker, *Boundary Element Techniques in Engineering*. Newnes Butterworths, London (1980).
16. C. A. Brebbia, J. C. F. Telles and L. C. Wrobel, *Boundary Element Techniques*. Springer, Berlin (1984).

ANALYSE THERMIQUE DE SENSIBILITE A LA FORME PAR UNE METHODE TRIDIMENSIONNELLE D'ELEMENT DE FRONTIERE

Résumé—On présente une analyse de sensibilité à la forme (DSA) très efficace et précise numériquement pour la réponse thermique d'un solide tridimensionnel (3D); elle utilise une formulation d'analyse directe d'élément de frontière (BEA). On présente les formulations théoriques des sensibilités pour la réponse primaire (température et flux normal thermique pariétaux) et des sensibilités à la réponse secondaire (composantes tangentielles du flux thermique, température et composantes du flux thermique en un point intérieur). On discute les données du calcul pour l'efficacité globale d'implémentation de ces formulations. Des résultats numériques sont présentés pour démontrer la précision et l'efficacité de cette approche.

UNTERSUCHUNG DER SENSITIVITÄT DER THERMISCHEN DARSTELLUNG EINES DREIDIMENSIONALEN RANDELEMENTS

Zusammenfassung—Für die Darstellung des thermischen Übergangsverhaltens eines dreidimensionalen Festkörpers wird eine recheneffiziente und genaue Sensitivitätsanalyse vorgestellt, die eine direkte und singuläre Formulierung der Randelementanalyse benutzt. Die theoretische Formulierung für die Sensitivität der primären Systemantwort (Oberflächentemperatur und Wärmestromdichte in normaler Richtung) und der sekundären Systemantwort (Tangentialkomponenten des Wärmestromdichten-Vektors, Temperatur und Komponenten des Wärmestromdichten-Vektors im Inneren) wird vorgestellt. Hierzu wird eine Anzahl von Rechenergebnissen bezüglich der Gesamteffizienz der Implementierung dieser Formulierungen diskutiert. Zur Darstellung der Genauigkeit und Effizienz dieses Näherungsverfahrens werden numerische Ergebnisse präsentiert.

АНАЛИЗ УПРАВЛЯЕМОСТИ ТЕПЛОВЫМ ПРОФИЛЕМ ТРЕХМЕРНОГО ГРАНИЧНОГО ЭЛЕМЕНТА

Аннотация—На основе прямого сингулярного анализа граничного элемеита предложен эффективный и точный метод анализа управляемости формой для определения динамических характеристик трехмерных твердых тел. Даны теоретические формулировки первичной управляемости характеристиками (температурой поверхности и пормальным тепловым потоком) и вторичной управляемости характеристиками (тангенциальными компонентами вектора теплового потока, температурой внутренней точки и компонентами вектора теплового потока). Обсуждается ряд расхождений в эффективности использования этих формулировок. Представлены численные результаты, подтверждающие точность и эффективность метода.